Attachment 5
PG&E Letter DCL-14-051

# AREVA Calculation No. 32-9221082-001

# Diablo Canyon Unit 2 Pressurizer Spray Nozzle Laminar Flaw Analysis – Non Proprietary

AREVA

# CALCULATION SUMMARY SHEET (CSS)

Document No. 32 - 9221082 - 001

Safety Related: ☒Yes ☐ No

Title Diablo Canyon Unit 2 Pressurizer Spray Nozzle Laminar Flaw Analysis – Non Proprietary

PURPOSE AND SUMMARY OF RESULTS:

Purpose

An inservice inspection of Diablo Canyon Power Plant (DCPP) Unit 2 overlaid Pressurizer (PZR) Spray nozzle revealed the existence of indications. The indications are described in the Diablo Canyon Power Plant Design Input Transmittal (DIT) summarized in Reference [1]. Previous disposition of all reported laminar indications per the rules of the acceptance standards Table IWB-3514-3 of ASME B&PV Code Section XI [2] and Section III [3] are reported in Reference [4]. The purpose of this document is to validate that the acceptance standards under IWB-3500 remain valid after any potential crack growth.

All indications observed in the PZR Spray nozzle are laminar. This document analyzes the indications for the remaining 38 years of plant operation. The indications are all embedded within the body of the nozzle and weld overlay. Therefore, no primary water stress corrosion crack growth mechanism would occur. The only mechanism by which indications could grow is fatigue crack growth.

This document provides a description of the indications, postulated flaws, applicable fatigue crack growth laws, fatigue crack growth analysis, and finally the predicted final flaw sizes are evaluated in accordance with the rules of ASME B&PV Code Section XI [2] and Section III [3]. Reference [5] Section 4.6, item 3 states that the applicable ASME code year is 2004 with addenda through 2005.

This document is the Non-Proprietary document of 32-9213780-002.

The purpose of Revision 001 is to address measurement uncertainty.

Summary of Results

The final crack sizes for all path cases are summarized in Table 7-5. The flaw area evaluation and overlay length evaluation are performed in Table 7-6 and Table 7-7, respectively. It is concluded that the laminar flaws meet the acceptance standards of Section XI of the ASME Code [2] for the remaining 38 years of plant operation.

Measurement uncertainty is Addressed in Appendix A. It is concluded in Appendix A that the laminar indications, including Indications 1 and 4 (Group 1) will not impact the integrity of the SWOL for 38 years of plant operation.

THE FOLLOWING COMPUTER CODES HAVE BEEN USED IN THIS DOCUMENT:

| CODE/VERSION/REV | CODE/VERSION/REV |
|---|---|
| None | |
| | |

THE DOCUMENT CONTAINS ASSUMPTIONS THAT SHALL BE VERIFIED PRIOR TO USE

☐Yes

☒ No

Diablo Canyon Unit 2 Pressurizer Spray Nozzle Laminar Flaw Analysis – Non Proprietary

Review Method: ☒ Design Review (Detailed Check)

☐ Alternate Calculation

## Signature Block

| Name and Title (printed or typed) | Signature | P/R/A and LP/LR | Date | Pages/Sections Prepared/Reviewed/Approved |
|---|---|---|---|---|
| Silvester J Noronha<br>Principal Engineer | [signature] | P | 5/29/14 | All. |
| Ashok D. Nana<br>Supervisory Engineer | [signature] | R | 5/30/14 | All. |
| Tim M Wiger<br>Engineering Manager | [signature] D.Kim for T.Wiger | A | 5/30/14 | All. |
| | | | | |

Note: P/R/A designates Preparer (P), Reviewer (R), Approver (A);
LP/LR designates Lead Preparer (LP), Lead Reviewer (LR)

### Project Manager Approval of Customer References (N/A if not applicable)

| Name (printed or typed) | Title (printed or typed) | Signature | Date |
|---|---|---|---|
| N/A | N/A | N/A | N/A |

### Mentoring Information (not required per 0402-01)

| Name (printed or typed) | Title (printed or typed) | Mentor to: (P/R) | Signature | Date |
|---|---|---|---|---|
| N/A | N/A | N/A | N/A | N/A |
| | | | | |

## Record of Revision

| Revision No. | Pages/Sections/Paragraphs Changed | Brief Description / Change Authorization |
|---|---|---|
| 000 | All | Original Release |
| 001 | Page 1 | Added purpose and summary for Revision 001 |
| | Section 5.0 | Listed new file |
| | Appendix A | Added Appendix A |
| | | |
| | | |
| | | |
| | | |
| | | |
| | | |
| | | |
| | | |
| | | |
| | | |
| | | |
| | | |
| | | |
| | | |
| | | |
| | | |
| | | |
| | | |
| | | |

## Table of Contents

Page

## Table of Contents
**(continued)**

## List of Tables

## List of Figures

## 1.0 INTRODUCTION

An inservice inspection of Diablo Canyon Power Plant (DCPP) Unit 2 overlaid Pressurizer (PZR) Spray nozzle revealed the existence of indications. The indications are described in the Diablo Canyon Power Plant Design Input Transmittal (DIT) documented in Reference [1]. All indications found in the PZR Spray nozzle are laminar. Previous disposition of the as found laminar indications per the rules of the acceptance standards in Table IWB-3514-3 of the ASME B&PV Code Section XI [2] and Article NB-3227.2 of ASME B&PV Code Section III [3] are documented in Reference [4]. Reference [4] did not consider any potential flaw growth that may occur due to sustained and cyclic operating conditions.

The purpose of this document is to assess the flaw growth that could take place for the remaining 38 years of plant operation. Because the laminar indications are located between the overlay and the original underlying materials, the surfaces of the indications do not come in contact with the reactor coolant. Therefore, no primary water stress corrosion crack (PWSCC) growth mechanism would occur. The only credible mechanism by which the indications could grow is fatigue crack growth.

This document provides a description of the indications, postulated flaws, applicable fatigue crack growth laws, fatigue crack growth analysis, and finally the predicted final flaw sizes are evaluated in accordance with the rules of ASME B&PV Code Section XI [2] and Section III [3]. Reference [5] Section 4.6, item 3 states that the applicable ASME code year is 2004 with addenda through 2005.

## 2.0 ANALYTICAL METHODOLOGY

This document performs flaw evaluation for dispositioning the NDE found indication in the DCPP PZR Spray nozzle. As described in Reference [1], all indications were laminar in nature. Thus, this document postulates cylindrical flaws to analyze all laminar indication.

For each postulated flaw, the flaw evaluation methodology consists of performing fatigue flaw growth for the specified service life. At the end of life, a flaw evaluation is performed to evaluate the end of life flaw acceptability.

This analysis postulated cylindrical sub-surface flaws, which could propagate by fatigue crack growth through the body of the Spray nozzle and full structural weld overlay (FSWOL). A linear elastic fracture mechanics (LEFM) analysis was performed to determine the applied stress intensity factors (SIFs) for the laminar flaw indications. The center-cracked panel (CCP) model was used with the radial and shear stresses to compute stress intensity factors for the laminar flaw indications. Flaw growth in the axial direction to estimate final flaw width was calculated using the SIF from the CCP model. Circumferential crack growth for estimating the final flaw length was evaluated by extending the flaw length in proportion to the ratio of final flaw width to the initial flaw width.

It should be noted that the planar flaw analysis for DCPP Unit 2 PZR nozzles [6] used 38 years of remaining service life. The current analysis was performed using the 38 years of remaining service life as well. The crack growth analysis considered the growth of embedded flaws due to cyclic loadings under the presence of residual stress from the welding processes. The final flaw sizes were calculated using the same operating transients considered in the original 2007 flaw growth analysis [7]. The predicted final flaw sizes were evaluated in accordance with the rules of ASME B&PV Code Section XI Table IWB-3514-3 [2]. Using Section III article NB-3227.2 [3], the presence of the laminar flaws was evaluated to assess the ability of the weld overlay to perform its intended function. Section III article NB-3227.2 [3] was used to verify that the weld overlay length excluding the indications is sufficient to transfer the load through shear back to the base metal considering a 100% through wall crack in the PWSCC susceptible material.

The initial structural overlay analysis was performed in 2007 per ASME Section III Subsection NB Code with 2001 and 2003 Addenda. During relief request of 2013, the shear stress check for the laminar flaw analysis was performed per ASME Section III Subsection NB Code with 2004 and 2005 Addenda. Both Code years were reviewed and it was determined that the criteria for pure shear stress evaluation per NB-3227.2 are the same. Hence, it is concluded that both the Codes are applicable to the current analyses and no additional reconciliation is required.

The remainder of this section describes the model used to calculate the stress intensity factor (SIF), crack growth calculation procedure, flaw evaluation, FSWOL minimum length requirement evaluation, and a list of the abbreviations and parameters used throughout the document.

### 2.1 Stress Intensity Factor Model

To calculate the stress intensity factor for the laminar flaw, the closed-form SIF solution from page 40 of Reference [8] for CCP model was used. The Mode I and Mode II configurations are illustrated in Figure 2-1.

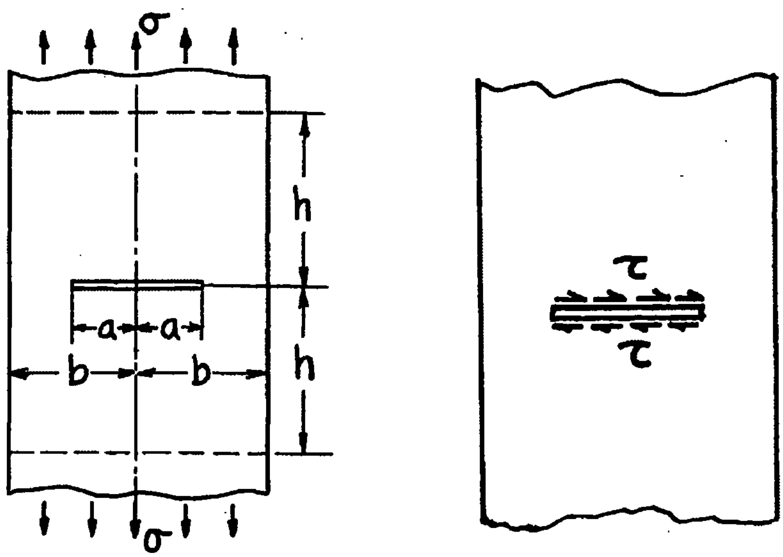


(Mode I) (Mode II)

**Figure 2-1: A Through-Wall Crack in the Center of a Plate**

For Mode I configuration, the $K_I$ solution is listed below:

$$K_I = \sigma\sqrt{\pi a} \cdot F\left(a/b\right)$$

$$F\left(a/b\right) = \left[1 - 0.025\left(a/b\right)^2 + 0.06\left(a/b\right)^4\right]\sqrt{\sec\frac{\pi a}{2b}}$$

Where, σ = uniform tensile stress

2a = crack length

2b = plate width

For Mode II configuration, the $K_{II}$ solution is identical to the Mode I solution except using τ (uniform shear stress) instead of σ (uniform tensile stress). It should be noted that some geometry idealization was made to use the CCP model SIF solution to analyze the Spray nozzle laminar indications. More discussion about the geometry idealization is provided in Section 4.1.

The functions F(a/b) is a geometry correction factor in which the b parameter accounts for the free surface effects. For an a/b value of 0, F(0)=1 and for an a/b value of 1, the geometry correction factor F(a/b) asymptotically approaches a very large value. For an a/b value of 99.9%, F(0.999) = 26.1. The selection of the b parameter should be based on the location of the closest free boundary to the analyzed flaw. Considering the Spray nozzle geometry, the b parameter can be quite large. The b parameter selection is further discussed in Section 4.1.

## 2.2 Fatigue Crack Growth Calculation

The steps to perform fatigue crack growth calculation are presented below. Note that the analysis assumed 360° laminar flaw, which is very conservative. Since the full circumference was assumed cracked; this section evaluated fatigue crack growth in the axial direction only.

1. For the first transient, Calculate the mode I maximum and minimum stress intensity factors ($K_{Imax}$ and $K_{Imin}$) based on the maximum radial stress $\sigma_{x\_max}$ and minimum radial stress $\sigma_{x\_min}$ in the first transient, respectively. Crack width (2*a*) and plate width (2*b*) are also required to calculate the SIF.
2. Calculate the stress intensity factor range due the radial stress ($\Delta K_I = K_{Imax} - K_{Imin}$).
3. Calculate the mode II maximum and minimum stress intensity factors ($K_{IImax}$ and $K_{IImin}$) based on the maximum shear stress $\tau_{max}$ and minimum shear stress $\tau_{min}$ in the first transient, respectively. Crack width (2*a*) and plate width (2*b*) are also required to calculate the SIF.
4. Calculate the stress intensity factor range due the shear stress ($\Delta K_{II} = K_{IImax} - K_{IImin}$).
5. Combine the stress intensity factor ranges from steps 2 and 4 to calculate the effective stress intensity factor range ($\Delta K$) to be used in the crack growth analysis as $\Delta K = [(\Delta K_I)^2 + (\Delta K_{II})^2]^{0.5}$.
6. To account for mean stress effect, calculate an effective R ratio (R), which is evaluated as $R = 1 - \Delta K / K_{max}$ using $K_{max} = [(K_{Imax})^2 + (K_{IImax})^2]^{0.5}$ and $\Delta K = [(\Delta K_I)^2 + (\Delta K_{II})^2]^{0.5}$. The R ratio is used in the crack growth equations to account for mean stress effect as described in Section 4.8.
7. Calculate crack growth increment (2Δ*a)* based on ΔK, R, and number of cycles per year for the specific transient. Metal temperature is also required to determine the parameters in the crack growth rate equation.
8. Update crack length to find the crack length at the end of the transient ($2a_f = 2a_i + 2\Delta a$), where $2a_f$ is the crack length at the end of the transient, $2a_i$ is the crack length at the beginning of the transient, and 2Δa is the crack growth increment during the transient as calculated in Step 7.
9. Repeat steps 1 through 8 for transients 2 through 17 with the crack length at the end of transient 1 is used as the starting crack length for transient 2, the crack length at the end of transient 2 is used as the starting crack length for transient 3 and so on. The crack length at the end of the last transient is also the crack length at the end of one year.
10. Repeat steps 1 through 9 to find crack length at the end of subsequent years with the crack length at the end of the first year is used as the starting crack length for the second year, the crack length at the end of the second year is used as the starting crack length for the third year and so on. The process is repeated for the subsequent years for the 38 year design life.

## 2.3 Laminar Flaw Evaluation

Disposition of all reported laminar indications per the rules of the acceptance standards in Table IWB-3514-3 of ASME B&PV Code Section XI [2] are reported in Reference [4]. The same evaluation procedure was used in this document with the final crack length now updated with calculated crack growth for 38 years of plant operation. For indication area evaluation, the acceptance criterion is in Table IWB-3514-3 [2], which requires that

$$A = 0.75(w \times l) \leq 7.5\ in^2$$

where $A$ is the flaw area, $w$ and $l$ are flaw width and length.

## 2.4 Minimum Required Overlay Length Calculations

For overlay length evaluation, the length of the weld overlay is acceptable provided that the effective overlay length ($l_{eff}$) is greater than the required overlay length ($l_{req}$). The required overlay length ($l_{req}$) is the length of the weld overlay that is sufficient to transfer the load through shear back to the base metal. Conservatively a 100% through wall crack is considered in the PWSCC (primary water stress corrosion cracking) susceptible material. The formulation in this section provides the procedure used for evaluating the minimum overlay length requirement.

The cross-sectional area ($A_{net}$) and section modulus ($Z_{net}$) of the net section are calculated considering a 100% through wall crack in the PWSCC susceptible material as

$$A_{net} = \frac{\pi}{4}\left((D+2t)^2 - D^2\right)$$

$$Z_{net} = \frac{2 \times I_{net}}{(D+2t)} = \frac{2 \times \frac{\pi}{64}((D+2t)^4 - D^4)}{(D+2t)}$$

where $D$ is the OD of the nozzle base metal, and $t$ is the minimum weld overlay thickness.

The extreme fiber tensile stress is calculated based on the net section properties with faulted moment ($M$) and axial load ($F$).

$$\sigma_{net} = \frac{M}{Z_{net}} + \frac{F}{A_{net}}$$

Conservatively consider the maximum allowable shear stress for the faulted case to be 0.6Sm (see NB-3227.2, Reference [5]) although the faulted allowable shear stress is higher. A force balance on the FSWOL with the maximum shear stress at the interface gives

$$\sigma_{net} \times t = 0.6 S_m \, l_{req}$$

Solving for the required minimum overlay length, $l_{req}$, gives

$$l_{req} = \frac{\sigma_{net} \times t}{0.6 S_m}$$

The effective length, $l_{eff}$, of the weld overlay is

$$l_{eff} = l_{wol} - l_{flaw}$$

where $l_{wol}$ is the length of the weld overlay based on the design drawings for minimum thickness conditions and $l_{flaw}$ is the axial dimension of the laminar flaw. Thus the length of the weld overlay is acceptable provided that $l_{eff}$ is greater than $l_{req}$.

It is noted that the initial structural overlay analysis was performed in 2007 per ASME Section III Subsection NB Code with 2001 and 2003 Addenda. During relief request of 2013, the shear stress check for the laminar flaw analysis was performed per ASME Section III Subsection NB Code with 2004 and 2005 Addenda. Both Code years were reviewed and it was determined that the criteria for pure shear stress evaluation per NB-3227.2 are the same. Hence, it is concluded that both Codes are applicable to the current analyses and no additional reconciliation is required.

## 2.5 List of Abbreviations and Parameters

This section defines the various abbreviations and parameters used throughout the document.

***Abbreviations***

| | |
|---|---|
| *DCPP* | Diablo Canyon Power Plant |
| *PZR* | Pressurizer |
| *DIT* | Design Input Transmittal |
| *PWSCC* | Primary Water Stress Corrosion Crack |
| *NDE* | Non Destructive Examination |
| *FSWOL* | Full Structural Weld Overlay |
| *LEFM* | Linear Elastic Fracture Mechanics |
| *CCP* | Center-Cracked Panel Model |
| *SIF* | Stress Intensity Factor |
| *DE* | Design Earthquake |
| *DDE* | Double Design Earthquake |
| *OBE* | Operation Basis Earthquake |

***Parameters for crack growth analysis***

| | | |
|---|---|---|
| $2a$ | Flaw width in the axial direction used in crack growth calculations | (in) |
| $2b$ | Plate width parameter used in the CCP model SIF calculations | (in) |
| $K_I$ | Mode I stress intensity factor | (ksi√in / MPa√m) |
| $K_{II}$ | Mode II stress intensity factor | (ksi√in / MPa√m) |
| $K_{Imax}$ | Maximum Mode I stress intensity factor | (ksi√in / MPa√m) |
| $K_{Imin}$ | Minimum Mode I stress intensity factor | (ksi√in / MPa√m) |
| $K_{IImax}$ | Maximum Mode II stress intensity factor | (ksi√in / MPa√m) |
| $K_{IImin}$ | Minimum Mode II stress intensity factor | (ksi√in / MPa√m) |
| $\Delta K_I = K_{Imax} - K_{Imin}$ | Mode I stress intensity factor range | (ksi√in / MPa√m) |
| $\Delta K_{II} = K_{IImax} - K_{IImin}$ | Mode II stress intensity factor range | (ksi√in / MPa√m) |
| $\Delta K = [(\Delta K_I)^2 + (\Delta K_{II})^2]^{0.5}$ | Mixed mode stress intensity factor range | (ksi√in / MPa√m) |
| $K_{max} = [(K_{Imax})^2 + (K_{IImax})^2]^{0.5}$ | Mixed mode maximum stress intensity factor | (ksi√in / MPa√m) |
| $R = 1 - \Delta K / K_{max}$ | Mixed mode R ratio | |
| $\sigma_{op\ min}$ | Minimum operating radial stress | (psi) |
| $\sigma_{op\ max}$ | Maximum operating radial stress | (psi) |
| $\tau_{op\ min}$ | Minimum operating shear stress | (psi) |
| $\tau_{op\ max}$ | Maximum operating shear stress | (psi) |
| $\sigma_{x\ max}$ | Maximum radial stress | (psi) |
| $\sigma_{x\ min}$ | Minimum radial stress | (psi) |

| | | |
|---|---|---|
| $\sigma_{rs}$ | Residual radial stress | (psi) |
| $\tau_{rs}$ | Residual shear stress | (psi) |
| $\sigma_{max}$ | Maximum radial stress | (psi) |
| $\sigma_{min}$ | Minimum radial stress | (psi) |
| $\tau_{max}$ | Maximum shear stress | (psi) |
| $\tau_{min}$ | Minimum shear stress | (psi) |
| $2a_i$ | Initial flaw width | (in) |
| $2a_f$ | Final flaw width | (in) |
| $2\Delta a$ | Flaw growth increment | (in) |
| $\Delta N$ | Number of cycles per year for a given transient in one direction | (cycle/year) |

**Parameters used in indication area evaluation**

| | | |
|---|---|---|
| $A$ | Laminar indication area evaluation | ($in^2$) |
| $w$ | Flaw width used in the indication area evaluation | (in) |
| $l$ | Flaw length used in the indication area evaluation | (in) |

**Parameters for crack growth rate equations**

| | | |
|---|---|---|
| $da/dN$ | Crack growth rate | (in/cycle) |
| $n$ | Crack growth equation exponent | |
| $T$ | Temperature | (°F or °C) |
| $C_{A600}, C, Co, S, S_R$ | Coefficient in the crack growth equations | |
| $R$ | R ratio | |

**Parameters for required overlay length evaluation**

| | | |
|---|---|---|
| $A_{net}$ | Cross-sectional area of the weld overlay | ($in^2$) |
| $Z_{net}$ | Section modulus of the weld overlay | ($in^3$) |
| $\sigma_{net}$ | Tensile stress is calculated based on the net section properties with faulted moment | (psi) |
| $l_{req}$ | Required overlay length to transfer the load through shear back to the base metal | (in) |
| $l_{eff}$ | Effective length of the weld overlay | (in) |
| $l_{wol}$ | Length of the weld overlay based on the design drawing | (in) |
| $l_{flaw}$ | Axial dimension of the laminar flaw used in required overlay length assessment | (in) |
| $OD$ | Outer diameter | (in) |
| $D$ | Diameter (same as outer diameter) | (in) |
| $t$ | Thickness (weld overlay) | (in) |
| $F$ | Axial load | (lbf) |
| $M$ | Bending Moment | (in-lbf) |

## 3.0 ASSUMPTIONS

This section discusses the assumptions and modeling simplifications used in this document.

### 3.1 Unverified Assumptions

There are no assumptions that must be verified before the present analysis can be used to support the disposition of the Diablo Canyon Unit 2 PZR Spray nozzle laminar indications.

### 3.2 Justified Assumptions

1. For the case where the R ratio < 0 (or similarly $K_{min}$ < 0), the R ratio is set equal to zero and the full range of $\Delta K$ is used in the crack growth calculations. This is a conservative assumption since crack closure due to compressive stress field is ignored.
2. The analysis assumed 360° laminar flaw for axial fatigue crack growth calculations, which is a conservative assumption since the full circumference was assumed cracked.
3. Final circumferential flaw length was estimated by extending the flaw length in proportion to the ratio of the final flaw width to initial flaw width. This is a conservative assumption since flaw growth in the circumferential (length) direction is expected to be less than the flaw growth in the axial (width) direction.

### 3.3 Modeling Simplifications

1. Multiple laminar flaws in Reference [1] are combined into larger, bounding flaws and extended to include a complete 360° arc length for crack growth calculations. Conservatively, CCP model is used to represent the 360° laminar flaws.
2. The mode I and mode II were combined using the square root summation of squares (SRSS). This results in a more conservative crack growth estimation than the linear summation of the individual crack growth increments due mode I and mode II when the crack growth law exponent is equal to or greater than 2 (i.e. for crack growth law proportional to $\Delta K^n$, when n is equal to or greater than 2, combining mode I and Mode II using the SRSS method results in a conservative estimation of the crack growth increment).
3. The 2b parameter for analyzing indications 1 and 4 was defined as the distance between the point where the overlay meets the nozzle and the butter. This is a conservative value for estimating the SIF since it is much smaller than the distance between the indication and the free surfaces of the nozzle and the overlay.
4. The 2b parameter for analyzing indications 2 and 3 was defined as twice the distance between the center of the SS Weld and the point at which the design reflects the structural thickness at $(0.75[r\ t]^{1/2})$ from the toe of the weld where r is the outside radius and t is the nominal thickness. This is a conservative value for estimating the SIF since it is much smaller than the distance between the indication and the free surfaces of the nozzle and the overlay.
5. Contribution of the external loads to the fatigue crack growth of the laminar flaws analyzed in the current document was assumed to be negligible. This is an engineering judgment since the sustained external loads will have minimal contributions to the cyclical radial and shear stress components.

# 4.0 DESIGN INPUTS

## 4.1 Geometry

Figure 4-1 shows a schematic view of the PZR Spray nozzle with FSWOL (taken from Figure 5-1 of Reference [13]). The different parts/subcomponents of the PZR Spray nozzle are labeled in Figure 4-1.

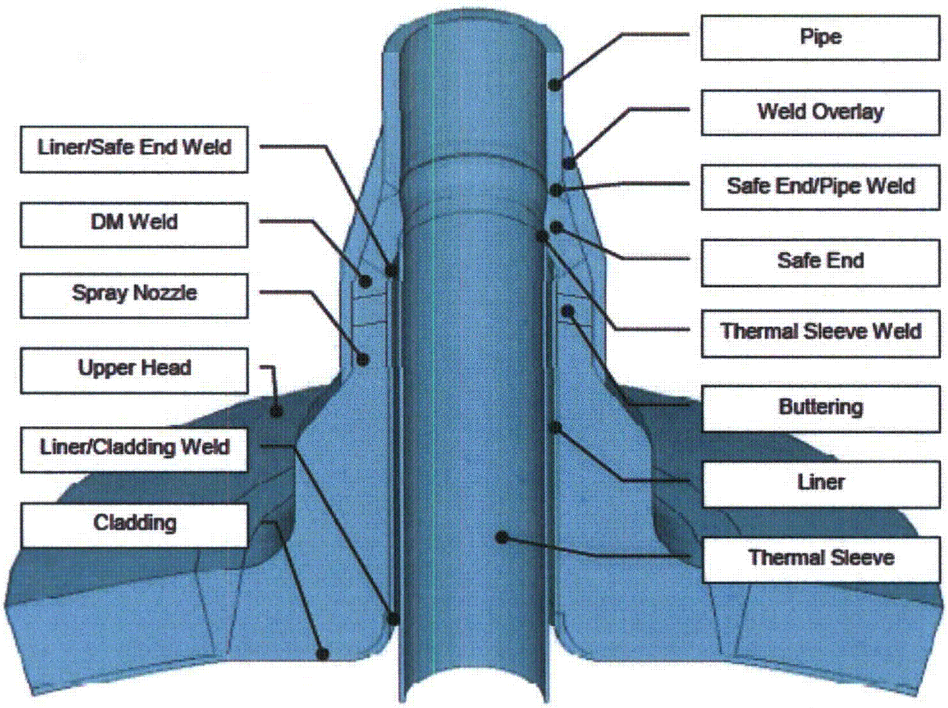


Figure 4-1: Schematic of the Spray Nozzle with FSWOL

Pertinent nozzle and overlay dimensions are estimated from references [9 and 10] and are shown in Table 4-1.

**Table 4-1: Spray Nozzle Dimensions**

[ ]

(1) Indications locations are shown in Figure 4-2 and Figure 4-3.

All PZR Spray nozzle indications are laminar with no planar content. The indications are located at the interface of the FSWOL and the original nozzle materials (nozzle and safe end/pipe weld). The indications detected in the PZR Spray nozzle are shown on Figure 4-2 and Figure 4-3, and with additional information provided in the Indication Data Sheet "WIB-345 OL Spray Nozzle" (Reference [1]). Detailed dimensions of the Spray nozzle are in Reference [9].

**Figure 4-2: WIB-345 Overlay Rollout Spray Nozzle (Ref. [1])**

**Figure 4-3: Spray Nozzle WIB-345 Overlay Indication Plot (Ref. [1])**

For the conservative 2D axisymmetric analysis in this document, the circumferential content of the laminar flaws were combined and extended to include a complete 360° arc length. The longitudinal (axial) content of the laminar flaws were combined according to the proximity rules of Section XI of the ASME Code.

Figure 4-4 shows idealization of the CCP Model to be used for the Spray nozzle indications. For the four Spray nozzle indications, the flaw dimensions and the 2b dimensions required for the SIF calculations are listed in Table 4-2.

**Table 4-2: Dimensions for SIF Calculation**

| Indication | Flaw Width 2a [(2)] (in) | 2b (in) | Flaw Length (in) | Materials |
|---|---|---|---|---|

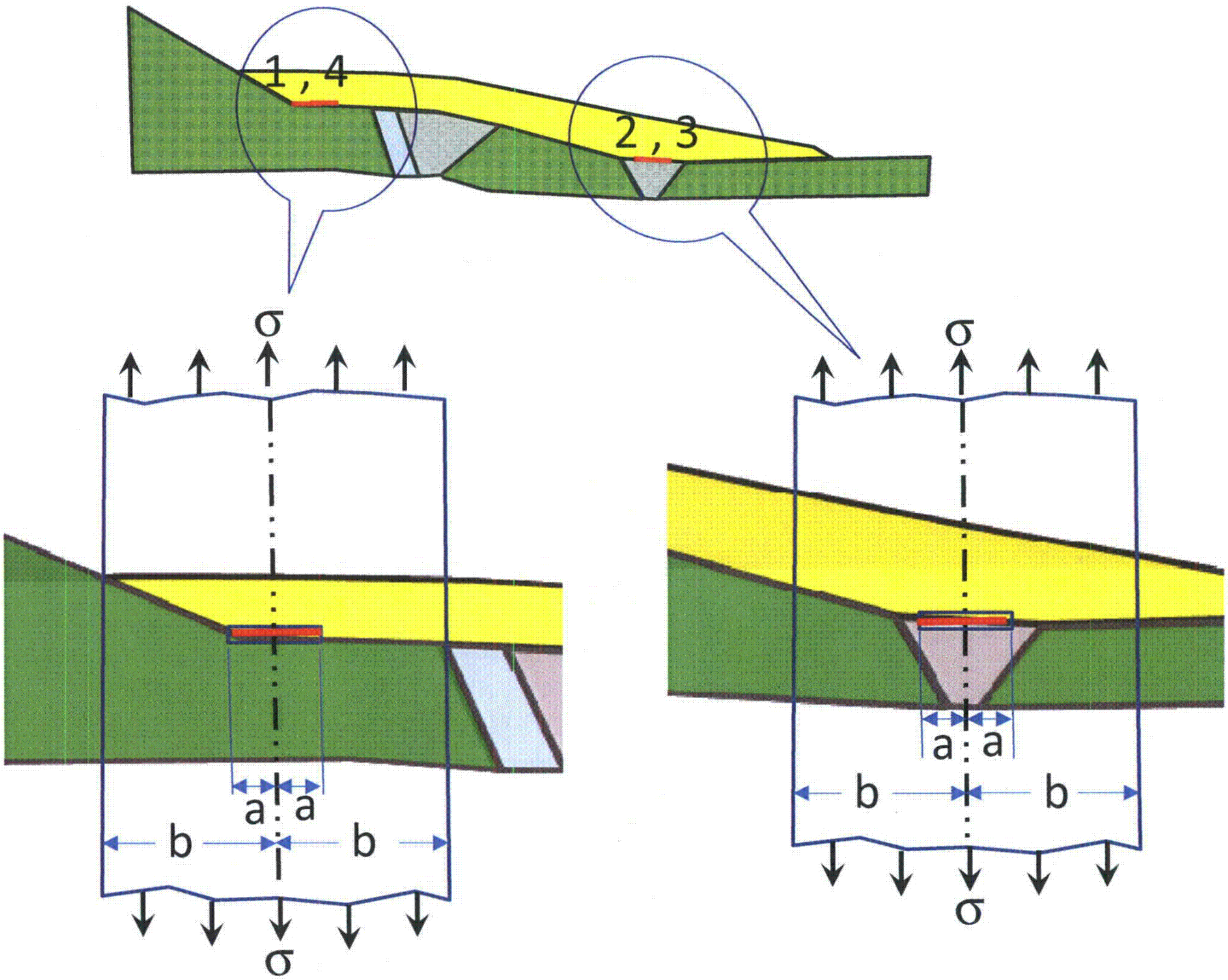


**Notes:**

[ ]

**Figure 4-4: Idealization of the CCP Model for the Spray Nozzle Indications**

### 4.2 Material

Reference [13] provides the material designations of various Spray nozzle components. The materials related to the path line cases investigated in this document are listed in Table 4-3.

**Table 4-3: Table of Materials**

[ ]

### 4.3 External Loads

Reference [7] lists the external piping loads that were used for the PZR Spray nozzle weld overlay original crack growth analysis. The crack growth loads applied at the safe end are presented in Table 4-4 and the crack growth loads at the nozzle are presented in Table 4-5. Note that these piping loads are not applicable to the fatigue crack growth of the laminar flaw analyzed in the current document because they have negligible contribution to the cyclical radial and shear stress components.

Reference [11] lists the external piping loads that were used for the PZR Spray nozzle weld overlay sizing calculations. The crack overlay sizing loads applied at the safe end are presented in Table 4-6 and overlay sizing loads at the nozzle are presented in Table 4-7. These loads were used for the minimum weld overlay length calculations performed in this document to evaluate the impact of the laminar flaws on the ability of the weld overlay to transfer the load through shear back to the base metal considering a 100% through wall crack in the PWSCC susceptible material.

**Table 4-4: PZR Spray Nozzle Sustained and Seismic Loading Conditions at Safe End Applicable to Crack Growth Analysis**

| Load Case | Forces (lbf) | Moments (in-lbf) |
|---|---|---|

[ ]

Note (1): The axial forces are aligned with the nozzle center line.

**Table 4-5: PZR Spray Nozzle Sustained and Seismic Loading Conditions at Nozzle Applicable to Crack Growth Analysis**

| Load Case | Forces (lbf) | Moments (in-lbf) |
|---|---|---|

[ ]

Note (1): The axial forces are aligned with the nozzle center line.

**Table 4-6: PZR Spray Nozzle Sustained and Seismic Loading Conditions at Safe End Applicable to Overlay Sizing**

| | Forces (lbf) | | | Moments (in-lbf) | | | |
|---|---|---|---|---|---|---|---|
| [ ] | [ ] | [ ] | [ ] | [ ] | [ ] | [ ] | [ ] |

[ ]

Note (1): The axial forces are aligned with the nozzle center line.

**Table 4-7: PZR Spray Nozzle Sustained and Seismic Loading Conditions at Nozzle Applicable to Overlay Sizing**

| Load Case | Forces (lbf) | | | Moments (in-lbf) | | | |
|---|---|---|---|---|---|---|---|
| | Axial(1) | $F_y$ | $F_z$ | Torsion | $M_y$ | $M_z$ | SRSS |

Note (1): The axial forces are aligned with the nozzle center line.

## 4.4 Operating Transients

The final flaw sizes are calculated using the same operating transients considered in the original 2007 flaw growth analysis [7]. Per Reference [12], the number of RCS design transients is established for 60-year design life. The operating transients applicable to laminar flaw growth are listed in Table 4-8.

**Table 4-8: Operating Transients for PZR Spray Nozzle [7]**

| Transient Number | Designation | Transient Name | Design Cycles |
|---|---|---|---|

| Transient Number | Designation | Transient Name | Design Cycles |
|---|---|---|---|

Notes:

(1) Seismic loading is part of the upset loading conditions. It is not expected to contribute to the radial and shear stress components, which constitute the crack driving force for laminar flaw. Thus, Seismic loading is not considered in fatigue crack growth of laminar flaws.

### 4.5 Operating Stresses

The cyclic operating stresses needed to calculate fatigue crack growth were obtained from a thermo elastic three-dimensional finite element analysis [13]. These fatigue stresses were developed for each of the transients at a number of time points to capture the maximum and minimum stresses due to fluctuations in pressure and temperature. The stresses that are required for crack growth analysis for the flaws are extracted in Appendix B of Reference [13]. Radial stresses contributing to Mode I crack growth are from files "SX". Shear stresses contributing to Mode II crack growth are from files "Sh". Since the SIF solutions in Section 2.1 are based on uniform stress, the stress data from Appendix B of Reference [13] were sorted to obtain maximum and minimum stresses along the path. These maximum and minimum stresses are conservatively used as the stress values for SIF calculation. In addition, the stress data were further sorted based on time points in each transient. The maximum and minimum stresses for all time points in each transient for the each path line case are tabulated in Table 4-9 through Table 4-10.

Reference [13] provided one set of results (stresses and temperatures) for analyzing indications #1 and #4 along pathline FLine2, as shown in Figure 4-5. Similarly, Reference [13] provided another set of results for analyzing indications #2 and #3 along pathline FLine4, as shown in Figure 4-5.

Since the indications in Figure 4-3 are located at the interfaces of different materials, it is not known which material the crack will grow into. Therefore, two cases were investigated for each pathline based on the two materials involved. Reference [13] defines two pathline cases, FL2_wol and FL2_noz for FLine2; the stresses for FL2_wol were extracted by selecting FSWOL material only and the stresses for FL2_noz were extracted by selecting nozzle material only. Similarly, for pathline FLine4 cases FL4_wol and FL4_wld were defined by selecting FSWOL material and weld material, respectively. This document calculates fatigue crack growths on these four cases.

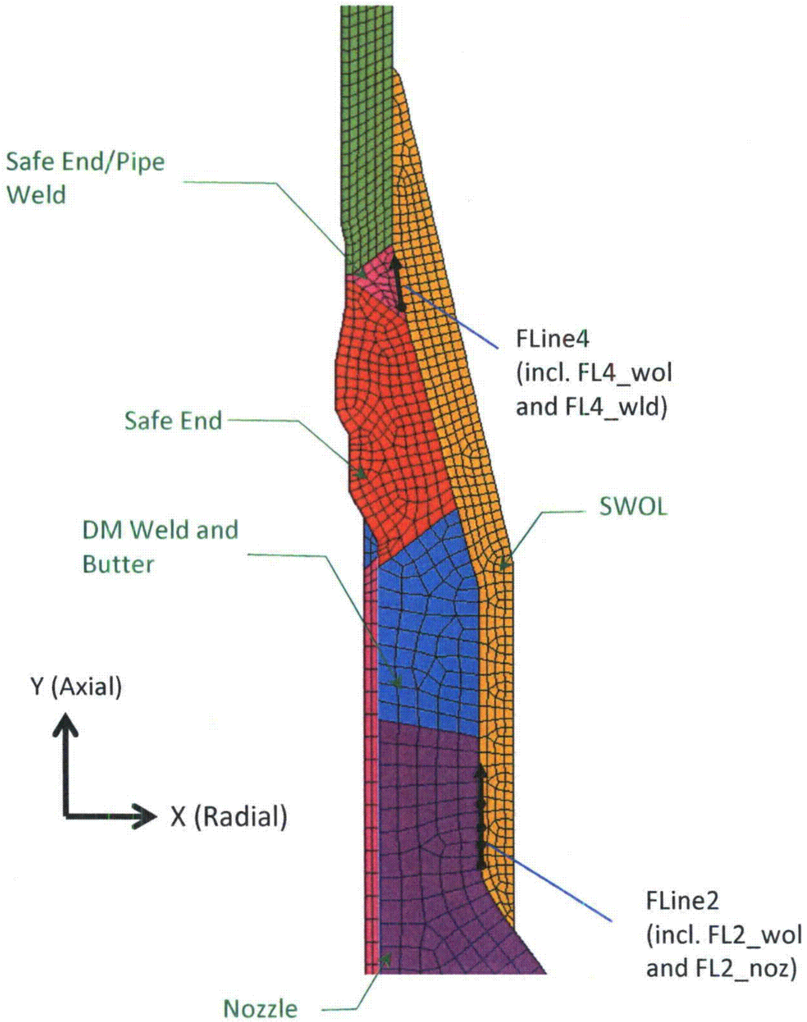


**Notes:**

- *Only laminar indications are found along pathlines FLine2 (indications 1 and 4) and Fline 4 (indications 2 and 3).*
- *FLine2 is path line used to sample results for evaluating laminar indications 1 and 4*
    - *FL2_wol used SWOL material for extracting stresses*
    - *FL2_noz used nozzle material for extracting stresses*
- *FLine4 is path line used to sample results for evaluating laminar indications 2 and 3*
    - *FL4_wol used SWOL material for extracting stresses*
    - *FL4_wld used weld material for extracting stresses*

**Figure 4-5: PZR Spray Nozzle with Path Lines Superposed**

### Table 4-9: Maximum and Minimum Stresses for Indications 1 and 4 (Pathline Fline2)

| Transient | Path Case FL2_wol | | | | Path Case FL2_noz | | | |
|---|---|---|---|---|---|---|---|---|
| | Minimum Radial Stress ($\sigma_{min}$) (ksi) | Maximum Radial Stress ($\sigma_{max}$) (ksi) | Minimum Shear Stress ($\tau_{min}$) (ksi) | Maximum Shear Stress ($\tau_{max}$) (ksi) | Minimum Radial Stress ($\sigma_{min}$) (ksi) | Maximum Radial Stress ($\sigma_{max}$) (ksi) | Minimum Shear Stress ($\tau_{min}$) (ksi) | Maximum Shear Stress ($\tau_{max}$) (ksi) |

[ ]

**Table 4-10: Maximum and Minimum Stresses for Indications 2 and 3 (Pathline Fline4)**

| Transient | Path Case FL4_wol | | | | Path Case FL4_wld | | | |
|---|---|---|---|---|---|---|---|---|
| | Minimum Radial Stress ($\sigma_{min}$) (ksi) | Maximum Radial Stress ($\sigma_{max}$) (ksi) | Minimum Shear Stress ($\tau_{min}$) (ksi) | Maximum Shear Stress ($\tau_{max}$) (ksi) | Minimum Radial Stress ($\sigma_{min}$) (ksi) | Maximum Radial Stress ($\sigma_{max}$) (ksi) | Minimum Shear Stress ($\tau_{min}$) (ksi) | Maximum Shear Stress ($\tau_{max}$) (ksi) |

[ ]

### 4.6 Operating Temperatures

Metal temperature is required for crack growth calculations. Metal temperatures along path lines were extracted in Appendix B of Reference [13] with file names "TH". The maximum temperatures along each pathline for all time points within each transient were determined to be used for crack growth calculation. Using the maximum temperature for fatigue crack growth calculation is conservative because higher temperatures result in higher crack growth rates based on the formulation given in Section 4.8. The maximum temperatures at all path cases during transients are tabulated in Table 4-11.

**Table 4-11: Maximum Temperatures for Path Line Cases (Units: °F)**

| Transient | Indications 1 and 4 (Pathline Fline2) | Indications 2 and 3 (Pathline Fline4) |
|---|---|---|

[ ]

### 4.7 Residual Stresses

Residual stresses due to [ ] are analyzed in Reference [14]. The residual stresses at the flaws investigated are extracted in Appendix C of Reference [14]. The minimum and maximum values from the bounding cases of radial and shear stresses are tabulated in Table 4-12. Residual stresses will be combined with operating stresses (Table 4-9 and Table 4-10) for SIF calculations.

**Table 4-12: Bounding Radial and Shear Weld Residual Stresses for Laminar Flaws**

| Location | | |
|---|---|---|
| | Radial Stress (ksi) | Shear Stress (ksi) |

[ ]

### 4.8 Fatigue Crack Growth Laws

Fatigue crack growth models for materials in Table 4-3 are described in the subsections below. Since the flaws in Figure 4-2 and Figure 4-3 do not come in contact with the reactor coolant, crack growth formulae that are applicable in the presence of air environment are used.

#### 4.8.1 [ ] (FSWOL)

The fatigue crack growth model for [ ] is obtained from Reference [15], which uses a multiplier of 2 upon those of Alloy 600. The crack growth rate (CGR) equation for Alloy 600 is given in NUREG/CR-6721 [16]. The CGR equation for [ ] is expressed as,

$$\left(\frac{da}{dN}\right)_{[\ \ ]} = 2 \cdot \left(\frac{da}{dN}\right)_{A600}$$

Substituting the Alloy 600 crack growth equation,

$$\left(\frac{da}{dN}\right)_{[\ \ ]} = 2 \cdot C_{A600} S_R (\Delta K)^n$$

Where ΔK is the stress intensity factor range in terms of MPa√m and da/dN is the crack growth rate in the units of meter/cycle. The other parameters are defined as,

$$C_{A600} = 4.835 \times 10^{-14} + 1.622 \times 10^{-16}\,T - 1.490 \times 10^{-18}\,T^2 + 4.355 \times 10^{-21}\,T^3$$

$$\Delta K = K_{max} - K_{min}$$

$$R = \frac{K_{min}}{K_{max}}$$

$$S_R = (1 - 0.82R)^{-2.2}$$

$$n = 4.1$$

T = metal temperature in °C

For the combined mode loading due to the opening mode (mode I) and sliding mode (mode II) the parameter $\Delta K$ was estimated as

$$\Delta K = (\Delta K_I^2 + \Delta K_{II}^2)^{0.5}$$

with $\Delta K_I$ and $\Delta K_{II}$ defined as.

$$\Delta K_I = K_{Imax} - K_{Imin}$$

$$\Delta K_{II} = K_{IImax} - K_{IImin}$$

Where $K_{Imax}$ and $K_{Imin}$ are the maximum and minimum mode I stress intensity factors, and $K_{IImax}$ and $K_{IImin}$ are the maximum and minimum mode II stress intensity factors.

a conservative estimation of the R ratio is given by

$$R = 1 - \Delta K / K_{max}$$

where $K_{max}$ is estimated as

$$K_{max} = (K_{Imax}^2 + K_{IImax}^2)^{0.5}$$

For the case where the R ratio < 0 (or similarly $K_{min}$ < 0), the R ratio is set equal to zero and the full range of $\Delta K$ is used in the crack growth calculations. This is a conservative assumption since crack closure due to compressive stress field is ignored.

### 4.8.2 Stainless Steel ( [ ] )

The fatigue crack growth model for stainless steel is obtained from Reference [2] Article C-8410. The CGR equation for stainless steel is expressed as,

$$\left(\frac{da}{dN}\right)_{SS-air} = C_0 (\Delta K)^n$$

Where $\Delta K$ is the stress intensity factor range in terms of ksi√in and da/dN is the crack growth rate in the units of in/cycle. The other parameters are defined as,

$$\Delta K = K_{max} - K_{min}$$

$$R = \frac{K_{min}}{K_{max}}$$

$$n = 3.3$$

$$C_0 = C \times S$$

$$C = 10^{\left(-10.009 + 8.12 \times 10^{-4} T - 1.13 \times 10^{-6} T^2 + 1.02 \times 10^{-9} T^3\right)}$$

$$S = \begin{cases} 1.0 \text{ when } R \le 0 \\ 1.0 + 1.8R \text{ when } 0 < R \le 0.79 \\ -43.35 + 57.97R \text{ when } 0.79 < R < 1.0 \end{cases}$$

T = metal temperature in °F

For the combined mode loading due to the opening mode (mode I) and sliding mode (mode II) the parameter $\Delta K$ was estimated as

$$\Delta K = (\Delta K_I^2 + \Delta K_{II}^2)^{0.5}$$

with $\Delta K_I$ and $\Delta K_{II}$ defined as

$$\Delta K_I = K_{Imax} - K_{Imin}$$

$$\Delta K_{II} = K_{IImax} - K_{IImin}$$

Where $K_{Imax}$ and $K_{Imin}$ are the maximum and minimum mode I stress intensity factors, and $K_{IImax}$ and $K_{IImin}$ are the maximum and minimum mode II stress intensity factors.

a conservative estimation of the R ratio is given by

$$R = 1 - \Delta K / K_{max}$$

where $K_{max}$ is estimated as

$$K_{max} = (K_{Imax}^2 + K_{IImax}^2)^{0.5}$$

#### 4.8.3 Low-Alloy Steel ( [ ] )

The fatigue crack growth model for low-alloy steel is obtained from Reference [2] Article A-4300. The CGR equation for low-alloy steel is expressed as,

$$\left(\frac{da}{dN}\right)_{LAS} = C_0 (\Delta K)^n$$

Where $\Delta K$ is the stress intensity factor range in terms of ksi√in and da/dN is the crack growth rate in the units of in/cycle. The other parameters are defined as,

$$R = \frac{K_{min}}{K_{max}}$$

$$\Delta K_{th} = \begin{cases} 5.0 & \text{for } R < 0 \\ 5.0(1 - 0.8R) & \text{for } 0 \le R < 1.0 \end{cases}$$

$$\text{For } 0 \le R \le 1, \begin{cases} S = 25.72(2.88 - R)^{-3.07} \\ \Delta K = K_{max} - K_{min} \end{cases}$$

$$\text{For } R < 0, \begin{cases} S = 1 \\ \Delta K = K_{max} - K_{min} \end{cases}$$

$$C_0 = \begin{cases} 0 & \text{for } \Delta K < \Delta K_{th} \\ 1.99 \times 10^{-10} S & \text{for } \Delta K \geq \Delta K_{th} \end{cases}$$

$$n = 3.07$$

Note that for the case where the R ratio < 0 (or similarly $K_{min} < 0$), it is assumed that $S = 1$ and $\Delta K = K_{max} - K_{min}$. This is a conservative assumption since crack closure due to compressive stress field is ignored.

For the combined mode loading due to the opening mode (mode I) and sliding mode (mode II) the parameter $\Delta K$ was estimated as

$$\Delta K = (\Delta K_I^2 + \Delta K_{II}^2)^{0.5}$$

with $\Delta K_I$ and $\Delta K_{II}$ defined as.

$$\Delta K_I = K_{Imax} - K_{Imin}$$

$$\Delta K_{II} = K_{IImax} - K_{IImin}$$

Where $K_{Imax}$ and $K_{Imin}$ are the maximum and minimum mode I stress intensity factors, and $K_{IImax}$ and $K_{IImin}$ are the maximum and minimum mode II stress intensity factors.

a conservative estimation of the R ratio is given by

$$R = 1 - \Delta K / K_{max}$$

where $K_{max}$ is estimated as

$$K_{max} = (K_{Imax}^2 + K_{IImax}^2)^{0.5}$$

## 5.0 COMPUTER USAGE

### 5.1 Software and Hardware

Mathcad [17] is used in this calculation. The hardware platform (Service Tag# 5VJV5S1) is Intel® Core™ i7-2640M CPU 2.80 GHz, 8.00 GB RAM. The operating system is Microsoft Windows 7 Enterprise, Copyright © 2009, Service Pack 1.

### 5.2 Computer Files

Table 5-1 lists the computes files used in this document. Files "*Spray.xlsm*" and "*spray.xmcd* " are from the previous revision of the document and were used to perform the calculations contained in the main body of the document. Only file "*spray_Uncertainty.xmcd* " was used in this revision, which contains the calculations performed in Appendix A. The computer files used in this document are available in AREVA ColdStor storage as indicated in Table 5-1.

**Table 5-1: Computer Files**

| File Name | Date & Time | Checksum | File Description |
|---|---|---|---|
| ColdStor location: \\cold\General-Access\32\32-9000000\32-9213780-002\official (revision 002 files) | | | |
| spray_Uncertainty.xmcd | Apr 29 2014 13:23:36 | 64547 | Mathcad file to calculate fatigue crack growth for all path lines for measurement uncertainty case. |
| ColdStor location: \\cold\General-Access\32\32-9000000\32-9213780-001\official (revision 001 files) | | | |
| Spray.xlsm | Mar 05 2014 15:42:31 | 02092 | Excel spreadsheets to verify crack growth calculation and perform laminar flaw qualification calculations |
| spray.xmcd | Mar 05 2014 15:42:11 | 50252 | Mathcad file to calculate fatigue crack growth for all path lines |

## 6.0 CALCULATIONS

The fatigue crack growth analysis methods outlined in Section 2.2 were used to calculate the final crack sizes for all cracks at the end of 38 years. A total of four cases (along two path lines) were analyzed in this document. All calculations were performed using Mathcad and Excel spreadsheet, as listed in Table 5-1. The remainder of this section contains sample calculations illustrating the fatigue crack growth analysis for each of the three materials considered in the current document ( [ ] , Stainless Steel, and Low Alloy Steel). In each sample calculation, detailed calculations are shown to illustrate fatigue crack growth increment for one transient. The manual calculations were repeated for all transients (not shown in the document) to assure that the manual calculations confirms the results for the first year as reported in Section 7.0.

### 6.1 [ ] (Weld Overlay)

Path line cases FL2_wol and FL4_wol are located at [ ] material. Using FL4_wol as an example, for transient #1 at the beginning of the first year,

<u>Given:</u>

| | | | | |
|---|---|---|---|---|
| $\sigma_{op\ min}$ | = | [ . ] | ksi | (Table 4-10) |
| $\sigma_{op\ max}$ | = | [ ] | ksi | (Table 4-10) |
| $\tau_{op\_min}$ † | = | [ ] | ksi | (Table 4-10) |
| $\tau_{op\_max}$ † | = | [ ] | ksi | Table 4-10) |
| $\sigma_{rs}$ | = | [ ] | ksi | (Table 4-12) |
| $\tau_{rs}$ | = | [ ] | ksi | (Table 4-12) |

Note †: conservatively using the largest magnitude of shear stress since the sign in shear only represents the direction of the stress.

| | | | | | | |
|---|---|---|---|---|---|---|
| 2a | = | [ ] | in | (Table 4-2) | | |
| 2b | = | [ ] | in | (Table 4-2) | | |
| T | = | [ ] | °F | (Table 4-11) | | |
| | = | [ ] | °C | | | |
| Number of Cycles 60 years | = | [ ] | cycles | (Table 4-8) | | |
| ΔN | = | [ ] | cycles/year | | | |
| $\sigma_{min} = \sigma_{op\_min} + \sigma_{rs}$ | = | [ ] | ksi | [ ] | MPa | |
| $\sigma_{max} = \sigma_{op\_max} + \sigma_{rs}$ | = | [ ] | ksi | [ ] | MPa | |
| $\tau_{min} = \tau_{op\_min} + \tau_{rs}$ | = | [ ] | ksi | [ ] | MPa | |
| $\tau_{max} = \tau_{op\_max} + \tau_{rs}$ | = | [ ] | ksi | [ ] | MPa | |

| | | | |
|---|---|---|---|
| a/b | = | [ ] | |
| $f(a/b) = (1-0.025(a/b)^2+0.06*(a/b)^4)\ [\sec(\pi a/2b)]^{0.5}$ | = | [ ] | |
| $K_{Imin} = \sigma_{max}\sqrt{(\pi a)}\ f(a/b)$ | = | [ ] | ksi√in |

| | | | | | | |
|---|---|---|---|---|---|---|
| $K_{Imax} = \sigma_{min}\sqrt{(\pi a)}\ f(a/b)$ | = | [ ] | ksi√in | | | |
| $K_{IImin} = \tau_{max}\sqrt{(\pi a)}\ f(a/b)$ | = | [ ] | ksi√in | | | |
| $K_{IImax} = \tau_{min}\sqrt{(\pi a)}\ f(a/b)$ | = | [ ] | ksi√in | | | |
| $\Delta K_I = K_{Imax} - K_{Imin}$ | = | [ ] | ksi√in | | | |
| $\Delta K_{II} = K_{IImax} - K_{IImin}$ | = | [ ] | ksi√in | | | |
| $\Delta K = (\Delta K_I^2 + \Delta K_{II}^2)^{0.5}$ | = | [ ] | ksi√in | = | [ ] | MPa√m |
| $K_{max} = (K_{Imax}^2 + K_{IImax}^2)^{0.5}$ | = | [ ] | ksi√in | | | |
| $R = 1 - \Delta K / K_{max}$ | = | [ ] | | | | |
| $S_R = (1 - 0.82\ R)^{-2.2}$ | = | [ ] | | | | |
| $C_{A600} = 4.835 \times 10^{-14} + 1.622 \times 10^{-16} \times T - 1.490 \times 10^{-18} \times T^2 + 4.355 \times 10^{-21} \times T^3$ | = | [ ] | | | | |
| $\Delta a = \Delta N(2\ C_{A600}\ S_R\ \Delta K^{4.1})$ | = | [ ] | m | = | [ ] | in |
| $2a = 2a + 2\ \Delta a$ | = | [ ] | in | | | |

The calculated 2a = [ ] is the initial 2a for the next transient crack growth calculation. After going through all 17 transients in the first year, the crack grows from [ ] to [ ], which confirms the results reported in Table 7-3 for the first year. Then, this [ ] is used as the initial crack length for the second year calculation and so on. Thus by repeating the process the final flaw size at the end of 38 years is obtained.

## 6.2 Stainless Steel (Pipe to Safe End Weld)

Path line case FL4_wld is located at stainless steel material. For transient #1 at the beginning of the first year,

**Given:**

| | | | | |
|---|---|---|---|---|
| $\sigma_{op\_min}$ | = | [ ] | ksi | (Table 4-10) |
| $\sigma_{op\ max}$ | = | [ ] | ksi | (Table 4-10) |
| $\tau_{op\_min}$ † | = | [ ] | ksi | (Table 4-10) |
| $\tau_{op\_max}$ † | = | [ ] | ksi | (Table 4-10) |
| $\sigma_{rs}$ | = | [ ] | ksi | (Table 4-12) |
| $\tau_{rs}$ | = | [ ] | ksi | (Table 4-12) |

Note †: switching the signs of maximum negative and positive shear stresses since the sign in shear only represents the direction of the stress.

| | | | | |
|---|---|---|---|---|
| 2a | = | [ ] | in | (Table 4-2) |
| 2b | = | [ ] | in | (Table 4-2) |
| T | = | [ ] | °F | (Table 4-11) |
| Number of Cycles 60 years | = | [ ] | | (Table 4-8) |
| $\Delta N$ | = | [ ] | cycles/year | |
| $\sigma_{min} = \sigma_{op\_min} + \sigma_{rs}$ | = | [ ] | ksi | |
| $\sigma_{max} = \sigma_{op\_max} + \sigma_{rs}$ | = | [ ] | ksi | |
| $\tau_{min} = \tau_{op\_min} + \tau_{rs}$ | = | [ ] | ksi | |
| $\tau_{max} = \tau_{op\_max} + \tau_{rs}$ | = | [ ] | ksi | |
| | = | | | |
| a/b | = | [ ] | | |
| $f(a/b) = (1-0.025(a/b)^2+0.06*(a/b)^4)\ [\sec(\pi a/2b)]^{0.5}$ | = | [ ] | | |
| $K_{Imin} = \sigma_{max}\sqrt{(\pi a)}\ f(a/b)$ | = | [ ] | ksi√in | |
| $K_{Imax} = \sigma_{min}\sqrt{(\pi a)}\ f(a/b)$ | = | [ ] | ksi√in | |
| $K_{IImin} = \tau_{max}\sqrt{(\pi a)}\ f(a/b)$ | = | [ ] | ksi√in | |
| $K_{IImax} = \tau_{min}\sqrt{(\pi a)}\ f(a/b)$ | = | [ ] | ksi√in | |
| $\Delta K_I = K_{Imax} - K_{Imin}$ | = | [ ] | ksi√in | |
| $\Delta K_{II} = K_{IImax} - K_{IImin}$ | = | [ ] | ksi√in | |
| $\Delta K = (\Delta K_I^2 + \Delta K_{II}^2)^{0.5}$ | = | [ ] | ksi√in | |
| $K_{max} = (K_{Imax}^2 + K_{IImax}^2)^{0.5}$ | = | [ ] | ksi√in | |
| $R = 1 - \Delta K / K_{max}$ | = | [ ] | | |
| S (Section 4.8.2) | = | [ ] | | |
| $C = 10^{\left(-10.009 + 8.12\times10^{-4}T - 1.13\times10^{-6}T^2 + 1.02\times10^{-9}T^3\right)}$ | = | [ ] | | |
| Co = CS | = | [ ] | | |
| $\Delta a = \Delta N(C_o\,\Delta K^{3.3})$ | = | [ ] | in | |
| $2a = 2a + 2\,\Delta a$ | = | [ ] | in | |

The calculated 2a = [ ] is the initial 2a for the next transient crack growth calculation. After going through all 17 transients in the first year, the crack grows from [ ] to [ ], which confirms the results reported in Table 7-4 for the first year. Then, this [ ] is used as the initial crack length for the second year calculation and so on. Thus by repeating the process the final flaw size at the end of 38 years is obtained.

### 6.3 Low-Alloy Steel ( [ ] Nozzle Material)

Path line case FL2_noz is located at low-alloy steel material. For transient #1 at the beginning of the first year,

**Given:**

| | | | | |
|---|---|---|---|---|
| $\sigma_{op\ min}$ | = | [ ] | ksi | (Table 4-9) |
| $\sigma_{op\ max}$ | = | [ ] | ksi | (Table 4-9) |
| $\tau_{op\_min}{}^{\dagger}$ | = | [ ] | ksi | (Table 4-9) |
| $\tau_{op\_max}{}^{\dagger}$ | = | [ ] | ksi | (Table 4-9) |
| $\sigma_{rs}$ | = | [ ] | ksi | (Table 4-12) |
| $\tau_{rs}$ | = | [ ] | ksi | (Table 4-12) |

Note $^{\dagger}$: conservatively using the largest magnitude of shear stress, which is from the maximum negative stress.

| | | | | |
|---|---|---|---|---|
| 2a | = | [ ] | in | (Table 4-2) |
| 2b | = | [ ] | in | (Table 4-2) |
| T | = | [ ] | °F | (Table 4-11) |
| Number of Cycles 60 years | = | [ ] | | (Table 4-8) |
| $\Delta N$ | = | [ ] | cycles/year | |
| $\sigma_{min} = \sigma_{op\_min} + \sigma_{rs}$ | = | [ ] | ksi | |
| $\sigma_{max} = \sigma_{op\_max} + \sigma_{rs}$ | = | [ ] | ksi | |
| $\tau_{min} = \tau_{op\_min} + \tau_{rs}$ | = | [ ] | ksi | |
| $\tau_{max} = \tau_{op\_max} + \tau_{rs}$ | = | [ ] | ksi | |

| | | | |
|---|---|---|---|
| a/b | = | [ ] | |
| $f(a/b) = (1-0.025(a/b)^2+0.06*(a/b)^4)\ [\sec(\pi a/2b)]^{0.5}$ | = | [ ] | |
| $K_{Imin} = \sigma_{max}\sqrt{(\pi a)}\ f(a/b)$ | = | [ ] | ksi√in |
| $K_{Imax} = \sigma_{min}\sqrt{(\pi a)}\ f(a/b)$ | = | [ ] | ksi√in |
| $K_{IImin} = \tau_{max}\sqrt{(\pi a)}\ f(a/b)$ | = | [ ] | ksi√in |
| $K_{IImax} = \tau_{min}\sqrt{(\pi a)}\ f(a/b)$ | = | [ ] | ksi√in |
| $\Delta K_I = K_{Imax} - K_{Imin}$ | = | [ ] | ksi√in |
| $\Delta K_{II} = K_{IImax} - K_{IImin}$ | = | [ ] | ksi√in |
| $\Delta K = (\Delta K_I{}^2 + \Delta K_{II}{}^2)^{0.5}$ | = | [ ] | ksi√in |
| $K_{max} = (K_{Imax}{}^2 + K_{IImax}{}^2)^{0.5}$ | = | [ ] | ksi√in |
| $R = 1 - \Delta K / K_{max}$ | = | [ ] | |
| $\Delta K_{th} =$ | = | [ ] | ksi√in |
| S (Section 4.8.3) | = | [ ] | |
| Co (Section 4.8.3) | = | [ ] | |
| $\Delta a = \Delta N(C_O \Delta K^{3.07})$ | = | [ ] | in |
| $2a = 2a + 2\ \Delta a$ | = | [ ] | in |

The calculated 2a = [ ] is the initial 2a for the next transient crack growth calculation. After going through all 17 transients in the first year, the crack grows from [ ] to [ ], which confirms the results reported in Table 7-2 for the first year. Then, this to [ ] is used as the initial crack length for the second year calculation and so on. Thus by repeating the process the final flaw size at the end of 38 years is obtained.

## 7.0 RESULTS

### 7.1 Fatigue Crack Growth

The crack sizes during 38 years of plant operations due to fatigue crack growth are presented in Table 7-1 through Table 7-4. The final crack sizes for all cases are summarized in Table 7-5. For indications 1 and 4 (considering cases FL2_noz and FL2_wol), the larger crack growth was observed for case FL2_noz. The final flaw size for indications 1 and 4 was estimated to be [ ] in. For indications 2 and 3 (considering cases FL4_wld and FL4_wol), the larger crack growth was observed for case FL4_wol. The final flaw size for indications 2 and 3 was estimated to be [ ] in. These two bounding crack sizes are used for laminar flaw evaluations in Section 7.2.

**Table 7-1: Fatigue Crack Growth for Indications 1 and 4 (Case FL2_wol)**

| Year | Year Start Crack Size (in.) | Crack Growth (in.) | Year End Crack Size (in.) |
|---|---|---|---|
| 1 | | | |
| 2 | | | |
| 3 | | | |
| 4 | | | |
| 5 | | | |
| 6 | | | |
| 7 | | | |
| 8 | | | |
| 9 | | | |
| 10 | | | |
| 11 | | | |
| 12 | | | |
| 13 | | | |

| Year | Year Start Crack Size (in.) | Crack Growth (in.) | Year End Crack Size (in.) |
|---|---|---|---|
| 14 | | | |
| 15 | | | |
| 16 | | | |
| 17 | | | |
| 18 | | | |
| 19 | | | |
| 20 | | | |
| 21 | | | |
| 22 | | | |
| 23 | | | |
| 24 | | | |
| 25 | | | |
| 26 | | | |
| 27 | | | |
| 28 | | | |
| 29 | | | |
| 30 | | | |
| 31 | | | |
| 32 | | | |
| 33 | | | |
| 34 | | | |
| 35 | | | |
| 36 | | | |
| 37 | | | |
| 38 | | | |

**Table 7-2: Fatigue Crack Growth for Indications 1 and 4 (Case FL2_noz)**

| Year | Year Start Crack Size (in.) | Crack Growth (in.) | Year End Crack Size (in.) |
|---|---|---|---|
| 1 | | | |
| 2 | | | |
| 3 | | | |
| 4 | | | |
| 5 | | | |
| 6 | | | |
| 7 | | | |
| 8 | | | |
| 9 | | | |
| 10 | | | |
| 11 | | | |
| 12 | | | |
| 13 | | | |
| 14 | | | |
| 15 | | | |
| 16 | | | |
| 17 | | | |
| 18 | | | |
| 19 | | | |
| 20 | | | |
| 21 | | | |
| 22 | | | |
| 23 | | | |
| 24 | | | |
| 25 | | | |
| 26 | | | |

| Year | Year Start Crack Size (in.) | Crack Growth (in.) | Year End Crack Size (in.) |
|---|---|---|---|
| 27 | | | |
| 28 | | | |
| 29 | | | |
| 30 | | | |
| 31 | | | |
| 32 | | | |
| 33 | | | |
| 34 | | | |
| 35 | | | |
| 36 | | | |
| 37 | | | |
| 38 | | | |

**Table 7-3: Fatigue Crack Growth for Indications 2 and 3 (Case FL4_wol)**

| Year | Year Start Crack Size (in.) | Crack Growth (in.) | Year End Crack Size (in.) |
|---|---|---|---|
| 1 | | | |
| 2 | | | |
| 3 | | | |
| 4 | | | |
| 5 | | | |
| 6 | | | |
| 7 | | | |
| 8 | | | |
| 9 | | | |
| 10 | | | |
| 11 | | | |
| 12 | | | |
| 13 | | | |
| 14 | | | |
| 15 | | | |
| 16 | | | |
| 17 | | | |
| 18 | | | |
| 19 | | | |
| 20 | | | |
| 21 | | | |
| 22 | | | |
| 23 | | | |
| 24 | | | |
| 25 | | | |
| 26 | | | |

| Year | Year Start Crack Size (in.) | Crack Growth (in.) | Year End Crack Size (in.) |
|---|---|---|---|
| 27 | | | |
| 28 | | | |
| 29 | | | |
| 30 | | | |
| 31 | | | |
| 32 | | | |
| 33 | | | |
| 34 | | | |
| 35 | | | |
| 36 | | | |
| 37 | | | |
| 38 | | | |

**Table 7-4: Fatigue Crack Growth for Indications 2 and 3 (FL4_wld)**

| Year | Year Start Crack Size (in.) | Crack Growth (in.) | Year End Crack Size (in.) |
|---|---|---|---|
| 1 | | | |
| 2 | | | |
| 3 | | | |
| 4 | | | |
| 5 | | | |
| 6 | | | |
| 7 | | | |
| 8 | | | |
| 9 | | | |
| 10 | | | |
| 11 | | | |
| 12 | | | |
| 13 | | | |
| 14 | | | |
| 15 | | | |
| 16 | | | |
| 17 | | | |
| 18 | | | |
| 19 | | | |
| 20 | | | |
| 21 | | | |
| 22 | | | |
| 23 | | | |
| 24 | | | |
| 25 | | | |
| 26 | | | |

| Year | Year Start Crack Size (in.) | Crack Growth (in.) | Year End Crack Size (in.) |
|---|---|---|---|
| 27 | | | |
| 28 | | | |
| 29 | | | |
| 30 | | | |
| 31 | | | |
| 32 | | | |
| 33 | | | |
| 34 | | | |
| 35 | | | |
| 36 | | | |
| 37 | | | |
| 38 | | | |

**Table 7-5: Summary of Fatigue Crack Growth**

| Indication | Case | Initial Crack Size (in.) | Final Crack Size (in.) | Growth (in.) | Crack Increase (%) |
|---|---|---|---|---|---|
| 1 and 4 | FL2_wol | [ ] | [ ] | [ ] | [ ] |
| | FL2_noz | [ ] | [ ] | [ ] | [ ] |
| 2 and 3 | FL4_wol | [ ] | [ ] | [ ] | [ ] |
| | FL4_wld | [ ] | [ ] | [ ] | [ ] |

### 7.2 Laminar Flaw Evaluation

The flaw area calculations are presented in Table 7-6. Based on the areas calculated in Table 7-6, it is concluded that the laminar flaws meet the laminar flaw acceptance criterion in article IWB-3514-3 of Section XI of the ASME Code [2] after 38 years of plant operation.

The minimum required overlay length evaluation is performed in Table 7-7. It is seen from Table 7-7 that the effective overlay length ($l_{eff}$), evaluated as the actual overlay length ($l_{wol}$) minus the flaw length ($l_{flaw}$), is greater than the minimum required overlay length ($l_{req}$), which is estimated based on Section III of the ASME Code [3]. Thus, it is concluded that the laminar flaws will not impact the overlay integrity after 38 years of plant operation.

**Table 7-6: Flaw Area Evaluation**

| | **Indications 1 and 4 (*1st Group*)** | **Indications 1 and 4 (*2nd Group*)** | **Indications 2 and 3** | **Reference/Comments** |
|---|---|---|---|---|
| *Initial flaw width* $w_{initial}$ (in.) | [ ] | [ ] (2) | [ ] | Table 4-2 |
| *Final flaw width* $w_{final}$ (in.) | [ ] | [ ] | [ ] | Table 7-5 |
| *Initial flaw length* $l_{initial}$ (in.) | [ ] | [ ] | [ ] | Table 4-2 |
| *Final flaw length*(1) $l_{final} = (w_{final} / w_{initial})\, l_{initial}$ (in.) | [ ] | [ ] | [ ] | |
| $A_{cal} = 0.75(w_{final} \times l_{final})$ (in$^2$) | [ ] | [ ] | [ ] | Section 2.3 |
| $A_{limit}$ (in$^2$) | [ ] | [ ] | [ ] | Table IWB-3514-3 of [2] |
| Check $A_{cal} \leq A_{limit}$ | OK | OK | OK | |

Notes

(1): Geometric similar flaw growth is assumed in the growth analysis. This assumption maintains a constant aspect ratio as defined by the initial flaw, $w_{initial}/l_{initial}$. The final flaw length, $l_{final}$ was computed based on $w_{final}$ determined in the growth analysis. The assumption of geometric flaw shape in the growth analysis is conservative since the cyclic stresses acting at the flaw plane are taken as uniform stress over the flaw area. Under uniform stress conditions, the flaw aspect ratio will decrease during growth making the $l_{final}$ smaller than that computed by the constant aspect ratio assumption.

(2): Actual flaw width for second group of indications 1 and 4 was listed in Table 4-2 to be [ ]. [ ] was conservatively used in the area evaluation.

**Table 7-7: Overlay Length Evaluation**

| Parameter | Indications 1 and 4 | Indications 2 and 3 | Reference/Comments |
|---|---|---|---|
| t (in) | | | |
| D (in) | | | |
| $Z_{net} = 2/(D+2t)\ (\pi/64)\ [(D+2t)^4 - D^4]$ (in³) | | | |
| $A_{net} = (\pi/4)\ [(D+2t)^2 - D^2]$ (in²) | | | |
| M (in-lbf) | | | |
| $M/Z_{net}$ (psi) | | | |
| F (lbf) | | | |
| $F/A_{net}$ (psi) | | | |
| $\sigma_{net} = M/Z_{net} + F/A_{net}$ (ksi) | | | |
| $S_m$ (ksi) | | | |
| $l_{req} = \sigma_{net}\ t / 0.6S_m$ (in) | | | |
| $l_{wol}$ (in) | | | |
| $l_{flaw}$ (in) | | | |
| $l_{eff} = l_{wol} - l_{flaw}$ (in) | | | |
| Check $l_{eff} > l_{req}$ | OK | OK | |

[ ]

## 8.0 REFERENCES


1. AREVA Document 38-9200149-001, "DCPP Unit 2 Pressurizer Nozzle NDE Data"
2. ASME Boiler and Pressure Vessel Code, Section XI, 2004 Edition with Addenda through 2005
3. ASME Boiler and Pressure Vessel Code, Section III, 2004 Edition with Addenda through 2005
4. AREVA Document 32-9199937-001, "DCPP Unit 2 - Evaluation of Laminar Indications on Pressurizer Nozzles"
5. "Safety Evaluation by the Office of Nuclear Reactor Regulation – Request for Relief from the American Society of Mechanical Engineers Boiler and Pressure Vessel Code, Section XI, Inservice Inspection Program, Pacific Gas and Electric Company, Diablo Canyon Power Plant, Unit No. 2 Docket No. 50- 323" Dated February 6, 2008 (ADAMS No. ML080110001)
6. AREVA Document 32-9199805-001, "Diablo Canyon Power Plant Unit 2 PZR Safety and Spray Nozzles Planar Flaw Analysis"
7. AREVA Document 32-9049064-001, "Diablo Canyon Unit 2 PZR Spray Nozzle Weld Overlay Crack Growth Evaluation"
8. Hiroshi Tada, Paul C. Paris, George R. Irwin, "The stress analysis of cracks handbook", 3rd edition, ASME, 2000
9. AREVA Drawing 02-8019233D-001, "Diablo Canyon Pressurizer Spray Nozzle Weld Overlay Design Input"
10. AREVA Drawing 02-8018400C-002, "Diablo Canyon Unit 2 Pressurizer Spray Nozzle Existing Configuration."
11. AREVA Document 32-9043546-001, "Diablo Canyon Unit 2, Pressurizer Spray Nozzle Weld Overlay Sizing Calculation"
12. AREVA Document 38-9046469-002, "DCPP 2 Pressurizer Nozzle Weld Overlay Design Data--Non-proprietary"
13. AREVA Document 32-9049112-003, "Diablo Canyon Unit 2 - Pressurizer Spray Nozzle Weld Overlay Structural Analysis"
14. AREVA Document 32-9049061-005, "Diablo Canyon Unit 2 Pressurizer Spray Nozzle Weld Overlay Residual Stress Analysis"

15. AREVA Document 32-9055891-006, "Fatigue and PWSCC Crack Growth Evaluation Tool AREVACGC"

16. NUREG/CR-6721, "Effects of Alloy Chemistry, Cold Work, and Water Chemistry on Corrosion Fatigue and Stress Corrosion Cracking of Nickel Alloys and Welds," U.S. Nuclear Regulatory Commission (Argonne National Laboratory), April 2001

17. Mathcad 15.0 Software, Parametric Technology Corporation, 140 Kendrick Street, Needham, MA 02494 USA

## APPENDIX A: FLAW SIZE UNCERTAINTY CONSIDERATION

This appendix contains a sensitivity analysis to account for NDE uncertainty in flaw size measurement. The NDE uncertainty was estimated in Reference [A.1] to be [ ] inch on either side of the flaw or [ ] inch total for the axial dimension of the laminar flaws. Incrementing the detected flaw sizes by [ ] inch, the flaw size to be used for flaw evaluation becomes [ ] inch for indications 1 and 4 and [ ] inch for indications 2 and 3. Using the updated flaw sizes, the crack growth analysis was performed following the procedure outlined in the main body of the document. The operating and residual stresses used for the crack growth analysis in this appendix are the same as the operating and residual stresses used in the main body of the document. The operating stresses used for the crack growth analysis are tabulated in Table 4-9 and Table 4-10 and the weld residual stresses are tabulated in Table 4-12. The path lines considered in the main body of the document are of sufficient lengths that they cover the [ ] inch uncertainty on either side of the laminar indications. The flaw growth evaluations were performed considering the design transients for the 38-year design life of the weld overlays. The results of the flaw growth analysis are tabulated in Table A-1.

**Table A-1: Results of Flaw Growth Analysis with [ ] in NDE Uncertainty**

| Indication | Case | Initial Crack Size (in.) | Final Crack Size (in.) | Growth (in.) | Crack Increase (%) |
|---|---|---|---|---|---|
| 1 and 4 | [ ] | [ ] | [ ] | [ ] | [ ] |
| | [ ] | [ ] | [ ] | [ ] | [ ] |
| 2 and 3 | [ ] | [ ] | [ ] | [ ] | [ ] |
| | [ ] | [ ] | [ ] | [ ] | [ ] |

The flaw area calculations are presented in Table A-2 and are based on increasing the width of the indications by [ ] inch to account for NDE sizing uncertainty. Based on these area calculations, it is concluded that the laminar indications in the second grouping for Indications 1 and 4, and Indications 2 and 3, meet the laminar flaw acceptance standards in Article IWB-3514.6 of Section XI of the ASME Code after 38 years of plant operation.

Indications 1 and 4 evaluated as Group 1 exceeds the allowable area limit of 7.5 $in^2$ ([ ] $in^2$ > 7.5 $in^2$) for this assessment. The Group 1 evaluation conservatively assumes the length of the indication to be continuous over 16.4 inches (using a smaller measurement uncertainty that is approximately 75% of the assumed [ ] inch increase in overall indication width will satisfy the acceptance standards of IWB-3514.6 (Table IWB-3514-3)).

**Table A-2: Laminar Area Evaluation with [ ] in NDE Uncertainty**

| | **Indications 1 and 4 (*1st Group*)** | **Indications 1 and 4 (*2nd Group*)** | **Indications 2 and 3** | **Reference/Comments** |
|---|---|---|---|---|
| *Initial flaw width* $w_{initial}$ (in.) | [ ] | [ ] (2) | [ ] | Table A-1 |
| *Final flaw width* $w_{final}$ (in.) | [ ] | [ ] | [ ] | Table A-1 |
| *Initial flaw length* $l_{initial}$ (in.) | [ ] | [ ] | [ ] | Table 4-2 |
| *Final flaw length*(1) $l_{final} = (w_{final} / w_{initial})\ l_{initial}$ (in.) | [ ] | [ ] | [ ] | |
| $A_{cal} = 0.75(w_{final} \times l_{final})$ (in$^2$) | [ ] (3) | [ ] | [ ] | Section 2.3 |
| $A_{limit}$ (in$^2$) | [ ] | [ ] | [ ] | Table IWB-3514-3 of [2] |
| Check $A_{cal} \leq A_{limit}$ | NO | YES | YES | |

Notes

(1): Geometric similar flaw growth is assumed in the growth analysis. This assumption maintains a constant aspect ratio as defined by the initial flaw, $w_{initial}/l_{initial}$. The final flaw length, $l_{final}$ was computed based on $w_{final}$ determined in the growth analysis. The assumption of geometric flaw shape in the growth analysis is conservative since the cyclic stresses acting at the flaw plane are taken as uniform stress over the flaw area. Under uniform stress conditions, the flaw aspect ratio will decrease during growth making the $l_{final}$ smaller than that computed by the constant aspect ratio assumption.

(2): Actual flaw width for second group of indications 1 and 4 was listed in Table 4-2 to be [ ]. [ ] (Including uncertainty) was conservatively used in the area evaluation.

(3): Note that this value is more than the area limit (7.5 in$^2$ ). However, on further analytical evaluation as permitted by IWB-3132.3, it is found to be acceptable as shown below.

To assess the significance of not meeting the NDE acceptance standards of IWB-3514.6 (Table IWB-3514-3), flaw acceptance was evaluated by analysis. Flaw acceptance by analytical evaluation is permitted by IWB-3132.3 when acceptance standards are exceeded. In this application, the analytical evaluation is based on Section III design rules to establish the allowable overlay weld length. The minimum required overlay length evaluation is summarized in Table A-3 where the effective overlay length ($l_{eff}$) is evaluated as the actual overlay length ($l_{wol}$) minus the flaw length ($l_{flaw}$). As seen in Table A-3, the overlay minimum length requirement is still satisfied for all flaws. For indications 1 and 4, the overlay minimum required length ($l_{req}$) is [ ] in, which is less than the effective overlay length ($l_{eff}$) of [ ]. For indications 2 and 3, the overlay minimum required length ($l_{req}$) is 0.76 in., which is less than the effective overlay length ($l_{eff}$) of [ ]. Thus, it is concluded that the laminar indications, including Indications 1 and 4 (Group 1) will not impact the integrity of the overlay for 38 years of plant operation.

**Table A-3: Overlay Length Evaluation with [ ] in NDE Uncertainty**

| Parameter | Indications 1 and 4 | Indications 2 and 3 | Reference/Comments |
|---|---|---|---|
| $l_{req} = \sigma_{net}\, t / 0.6S_m$ (in) | [ ] | [ ] | Table 7-7 |
| $l_{wol}$ (in) | [ ] | [ ] | Table 7-7 |
| $l_{flaw}$ (in) | [ ] | [ ] | Table A-1 |
| $l_{eff} = l_{wol} - l_{flaw}$ (in) | [ ] | [ ] | |
| Check $l_{eff} > l_{req}$ | YES | YES | |

**Conclusion**

The analysis presented above confirms that the SWOL with postulated flaws accounting for an NDE measurement uncertainty of [ ] inch on either side of the flaw or [ ] inch total for the axial dimension of the laminar flaws still meets the overlay length requirement per NB-3227.2[3] in Spray Nozzle. Thus, it is concluded that the laminar indications, including Indications 1 and 4 (Group 1) will not impact the integrity of the SWOL for 38 years of plant operation.

**References**

A.1. AREVA Document 38-9223975-000 “DCPP2 - NDE Measurement Uncertainty Information.”